

Magnetic Control and Real-Time Monitoring of Stem Cell Differentiation by the Ligand Nanoassembly

Sungkyu Lee, Myeong Soo Kim, Kapil D. Patel, Hyojun Choi, Ramar Thangam, Jinho Yoon, Thomas Myeongseok Koo, Hee Joon Jung, Sunhong Min, Gunhyu Bae, Yuri Kim, Seong-Beom Han, Nayeon Kang, Minjin Kim, Na Li, Hong En Fu, Yoo Sang Jeon, Jae-Jun Song, Dong-Hwee Kim, Steve Park, Jeong-Woo Choi, Ramasamy Paulmurugan, Yun Chan Kang, Heon Lee, Qiang Wei, Vinayak P. Dravid, Ki-Bum Lee,* Young Keun Kim,* and Heemin Kang*

Native extracellular matrix (ECM) exhibits dynamic change in the ligand position. Herein, the ECM-emulating control and real-time monitoring of stem cell differentiation are demonstrated by ligand nanoassembly. The density of gold nanoassembly presenting cell-adhesive Arg-Gly-Asp (RGD) ligand on Fe₃O₄ (magnetite) nanoparticle in nanostructures flexibly grafted to material is changed while keeping macroscale ligand density invariant. The ligand nanoassembly on the Fe₃O₄ can be magnetically attracted to mediate rising and falling ligand movements via linker stretching and compression, respectively. High ligand nanoassembly density stimulates integrin ligation to activate the mechanosensing-assisted stem cell differentiation, which is monitored via in situ real-time electrochemical sensing. Magnetic control of rising and falling ligand movements hinders and promotes the adhesion-mediated mechanotransduction and differentiation of stem cells, respectively. These rising and falling ligand states yield the difference in the farthest distance (≈ 34.6 nm) of the RGD from material surface, thereby dynamically mimicking static long and short flexible linkers, which hinder and promote cell adhesion, respectively. Design of cytocompatible ligand nanoassemblies can be made with combinations of dimensions, shapes, and biomimetic ligands for remotely regulating stem cells for offering novel methodologies to advance regenerative therapies.

1. Introduction

Dynamic movement of ligands, such as the cell adhesive tripeptide Arg-Gly-Asp (RGD) motif, is observed in native extracellular matrix (ECM).^[1] A variety of tissues, including tendons,^[2] intervertebral disks,^[3] and bone,^[4] present ligand nanostructures that can regulate the dynamic adhesion and differentiation of cells.^[5] Collagen ECM proteins that comprise the predominant population in native bone exhibit nanostructured RGD ligand.^[6] Controlling the movement of cell-adhesive ECM proteins regulates dynamic integrin-RGD ligation to mediate intracellular assembly of F-actin cytoskeleton and focal adhesion complexes that trigger mechanotransduction signals to facilitate stem cell differentiation.^[7] Designing ECM-mimicking materials with movement controllability of ligand nanostructures can assist the elucidation of dynamic nanoscale cell–material interplay to

S. Lee, K. D. Patel, H. Choi, R. Thangam, T. M. Koo, S. Min, G. Bae, Y. Kim, N. Kang, M. Kim, H. E. Fu, Y. C. Kang, H. Lee, Y. K. Kim, H. Kang
Department of Materials Science and Engineering
Korea University
Seoul 02841, Republic of Korea
E-mail: ykim97@korea.ac.kr; heeminkang@korea.ac.kr
M. S. Kim, R. Thangam
Institute for High Technology Materials and Devices
Korea University
Seoul 02841, Republic of Korea
J. Yoon, K.-B. Lee
Department of Chemistry and Chemical Biology
Rutgers University
Piscataway, NJ 08854, USA
E-mail: kblee@rutgers.edu

J. Yoon, J.-W. Choi
Department of Chemical and Biomolecular Engineering
Sogang University
Seoul 04107, Republic of Korea

H. J. Jung, V. P. Dravid
Department of Materials Science and Engineering
Northwestern University
Evanston, IL 60208, USA

H. J. Jung, V. P. Dravid
International Institute for Nanotechnology
Evanston, IL 60208, USA

H. J. Jung, V. P. Dravid
NUANCE Center
Northwestern University
Evanston, IL 60208, USA

S.-B. Han, D.-H. Kim
KU-KIST Graduate School of Converging Science and Technology
Korea University
Seoul 02841, Republic of Korea

 The ORCID identification number(s) for the author(s) of this article can be found under <https://doi.org/10.1002/sml.202102892>.

DOI: 10.1002/sml.202102892

regulate and monitor cell adhesion and differentiation in situ.^[8] The development of dynamic ECM-emulating materials^[9] with remote controllability can regulate dynamic cell–material interplay, respectively.^[10] Remotely activatable signals include light^[11] and magnetic fields.^[12]

Light irradiation can control ligand-tethered light-activatable materials^[13] but is limited due to high absorption of light, such as ultraviolet-light-controlled cell adhesion in vivo.^[14] The nanoscale presentation of bioactive ligand^[15] has been modulated on a planar array of largely static homogeneous ligand-tethered nanoparticles^[16] by changing spatial density and interparticle spacing,^[17] local versus macroscale density,^[18] clusters,^[19] ordering versus disordering,^[20] micropatterned nanoparticles,^[21] and among others. However, in these prior studies, the complex nature of ligand distribution in natural tissues was not presented. The nanoscale display of a bioactive ligand has been dynamically controlled by manipulating the movement of individual ligand-tethered magnetic nanoparticles via magnetic field,^[22] which is distinct from the integrated ligand nanostructures shown in this study.^[23] Recently, our group has demonstrated the magnetic manipulation of the linear alignment,^[24] expansion,^[25] and planar movement^[26] of the ligand to regulate cellular adhesion and differentiation. Furthermore, magnetic control of restricting ligand mobility suppressed colony development with cancer stem-like cell^[27] or promoted stem cell differentiation,^[28] which was also regulated by controlling ligand exposure.^[29]

Herein, we report the change of the density of a ligand-presenting gold nanoparticle assembly on a Fe₃O₄ (magnetite) nanoparticle (in “OFF” state) flexibly grafted to substrate using a flexible linker (**Scheme 1**).^[30] Magnetic field was applied to

attract the ligand nanoassembly on Fe₃O₄ to mediate rising (“Rising” ON, increasing vertical ligand position) and falling (“Falling” ON, decreasing vertical ligand position) nanoscale ligand movement via reversible stretching and compression of the flexible linker, respectively, to regulate the adhesion, mechanosensing, and differentiation of stem cells.

2. Results and Discussion

2.1. The Ligand Nanoassembly is Changeable on the Fe₃O₄

We prepared Fe₃O₄ nanoparticles of a size significantly larger than that of gold nanoparticles^[22] for nanoassembly on the surface of Fe₃O₄ nanoparticles. We facilitated nanoassembly through amino–silica functionalization to facilitate the assembly of gold nanoparticles on the Fe₃O₄ nanoparticles via amino–gold bonding (Figure S1, Supporting Information). Vibrating sample magnetometry revealed reversible magnetic property of Fe₃O₄ nanoparticles with a high saturation magnetization value of 671 emu g⁻¹ and nearly overlapping hysteresis curves (Figure S2, Supporting Information). We confirmed homogeneous amino–silica shell coating on the surface of the Fe₃O₄ core nanoparticles via transmission electron microscopy (TEM) imaging (Figure S3, Supporting Information). Dynamic light scattering (DLS) spectra confirmed that the diameter of the Fe₃O₄ nanoparticles coated with the amino–silica shell was 212 ± 15 nm (Figure S4, Supporting Information). Gold nanoparticles^[31] exhibited uniform size distribution with a diameter of 12.3 ± 0.6 nm (Figures S5 and S6, Supporting Information).

For change of the density of gold nanoparticles on the Fe₃O₄ nanoparticles in nanoassembly, we regulated the ratio of reaction volume (low, moderate, or high volume) of the gold nanoparticle suspension to that of the Fe₃O₄@amino–silica suspension to yield low, moderate, or high densities of the gold nanoparticle assembly on the Fe₃O₄ nanoparticle. High-angle annular dark-field STEM (HAADF-STEM) images revealed the atomic arrangement in crystalline Fe₃O₄ and gold nanoassembly in the assembled nanostructures with gradual increase in the low, moderate, and high densities of uniformly distributed gold nanoassembly on the Fe₃O₄ in the nanostructures (**Figure 1a**; Figure S7, Supporting Information). We quantified the surface areas of the nanoassembly per Fe₃O₄ nanoparticle as 20 494 ± 3154, 57 977 ± 3345, and 95 355 ± 6733 nm² for low, moderate, and high nanoassembly groups, respectively, which were significantly different (Figure 1b). We determined significantly different nanoassembly densities (the number of gold nanoassembly units per Fe₃O₄) as 39 ± 5, 109 ± 6, and 180 ± 13 for low, moderate, and high nanoassembly groups, respectively. UV–vis spectra revealed the presence of gold and Fe₃O₄ nanoparticles in all of nanoassembly groups (Figure 1c). DLS spectra revealed similar size distributions in nanoassembly groups at various densities (Figure 1d).

2.2. Magnetic Control of Movement of the Ligand Nanoassembly

For remote control of nanoscale ligand movement, we grafted a long flexible poly(ethylene glycol) (PEG) linker (*M_w*: 5 kDa) to the surface of the nanoassembly via the gold–thiol reaction

N. Li, J. Song
Department of Otorhinolaryngology-Head and Neck Surgery
Korea University College of Medicine
Seoul 08308, Republic of Korea

Y. S. Jeon
Institute of Engineering Research, Korea University
Seoul 02841, Republic of Korea

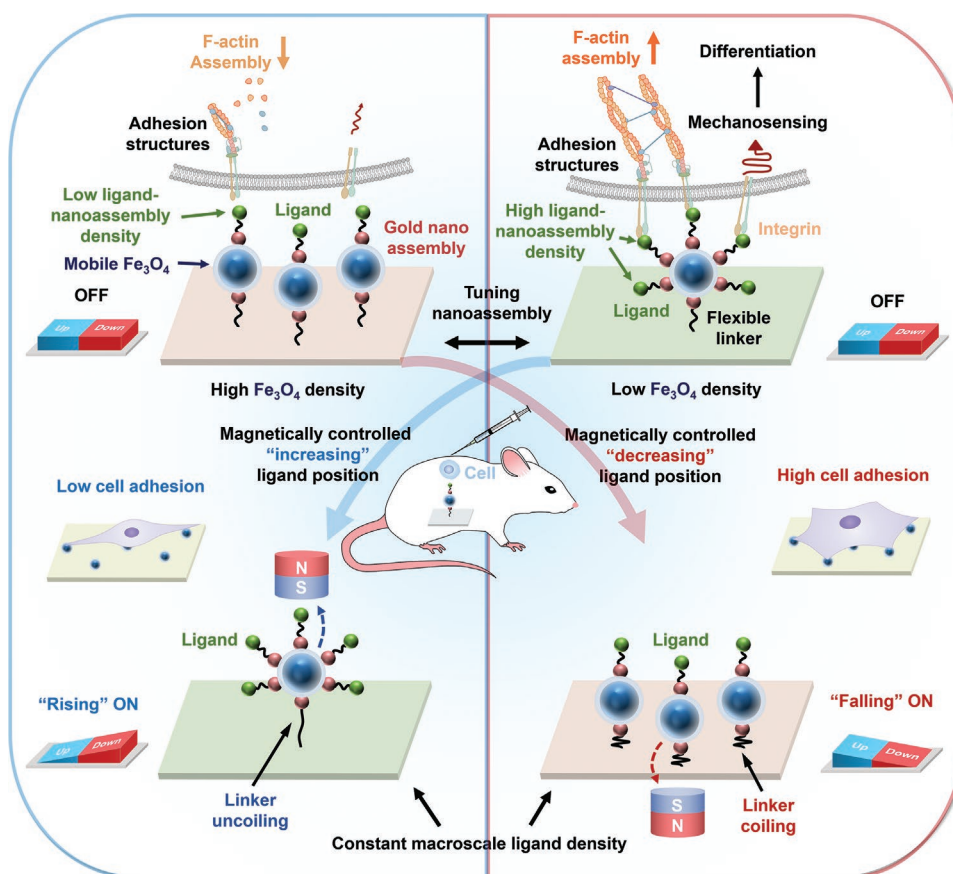
S. Park
Department of Materials Science and Engineering
Korea Advanced Institute of Science and Technology (KAIST)
Daejeon 34141, Republic of Korea

R. Paulmurugan
Department of Radiology
Molecular Imaging Program at Stanford
Stanford University School of Medicine
Stanford University
Palo Alto, CA 94304, USA

R. Paulmurugan
Department of Radiology
Canary Center at Stanford for Cancer Early Detection
Stanford University School of Medicine
Stanford University
Palo Alto, CA 94304, USA

Q. Wei
College of Polymer Science and Engineering
State Key Laboratory of Polymer Materials and Engineering
Sichuan University
Chengdu 610065, China

H. Kang
Department of Biomicrosystem Technology
Korea University
Seoul 02841, Republic of Korea



Scheme 1. Schematic summary of the experimental methodology in this study. A dynamic platform was developed by flexible grafting of ligand-tethered gold nanoassembly onto the Fe_3O_4 (via change of the nanoassembly density in “OFF” state) to substrate while keeping the macroscale ligand density invariant. Remote control of nanoscale ligand movement was achieved by magnetically attracting the ligand nanoassembly to mediate rising (“Rising” ON, increasing vertical ligand position) and falling (“Falling” ON, decreasing vertical ligand position) movements via stretching and compression of a flexible linker molecule, respectively. High ligand nanoassembly density enhanced the mechanosensing-aided differentiation of stem cells (as compared to the low ligand nanoassembly density). Magnetic manipulation of the “Rising” ON and “Falling” ON impeded and promoted the stem cell mechanosensing-mediated differentiation, respectively, thereby advancing regenerative therapies.

(Figure 1e; Figure S8, Supporting Information). To keep macroscale ligand density constant, various nanoassemblies on the Fe_3O_4 at increasing nanoassembly densities per Fe_3O_4 nanoparticle were grafted to an aminated substrate via 1-ethyl-3-(3-dimethylaminopropyl) carbodiimide/N-hydroxysuccinimide reaction at decreasing Fe_3O_4 densities. The activated flexible linker-coated nanoassembly on the substrate further reacted with amino-RGD peptide ligand to create ligand nanoassembly. Zeta potential analysis of nanoassemblies at various densities through serial surface modification processes using the PEG linker and RGD ligand revealed changes in surface charges, which confirmed the successful modification of the nanoassemblies (Figure S9, Supporting Information). We also confirmed successful chemical functionalization of ligand nanoassembly via the Fourier transform infrared (FTIR) spectroscopy analysis (Figure 1e; Figure S10a,b, Supporting Information).

Homogeneous grafting of various flexible linker-coated nanoassemblies at constant macroscale ligand density to the substrate was verified through scanning electron microscopy (SEM) imaging. The results showed decreasing substrate-grafted Fe_3O_4 nanoparticle densities (5.4 ± 0.2 , 2.3 ± 0.3 , and 1.3 ± 0.1

particles μm^{-2} for low, moderate, and high nanoassembly densities, respectively) with increasing nanoassembly densities (Figure 2a,b). We optimized substrate-grafted Fe_3O_4 densities with various ligand nanoassembly densities such that they efficiently regulate the focal adhesion, mechanosensing, and differentiation of stem cells. Macroscale ligand surface density exhibited similar values (between 110 600 and 131 300 $\text{nm}^2 \mu\text{m}^{-2}$) without significant differences (Figure 2b).

Remote control of integrated vertical nanoscale ligand movement via magnetic attraction of the ligand nanoassembly on the Fe_3O_4 nanoparticle was characterized via in situ atomic force microscopy (AFM) imaging under the magnetic field. We conducted serial in situ AFM imaging on the identical areas of ligand nanoassembly after placing a permanent magnet at the upper side of the substrate to induce the rising movement (“Rising” ON) of ligand nanoassembly via stretching of a flexible linker or at the lower side of the substrate to induce the falling movement (“Falling” ON) of ligand nanoassembly via compression of the flexible linker or without the magnet (“OFF”) (Figure 2c,d). Similar diameters of ligand nanoassembly in the “OFF,” “Rising” ON, and “Falling” ON states (between 214.8

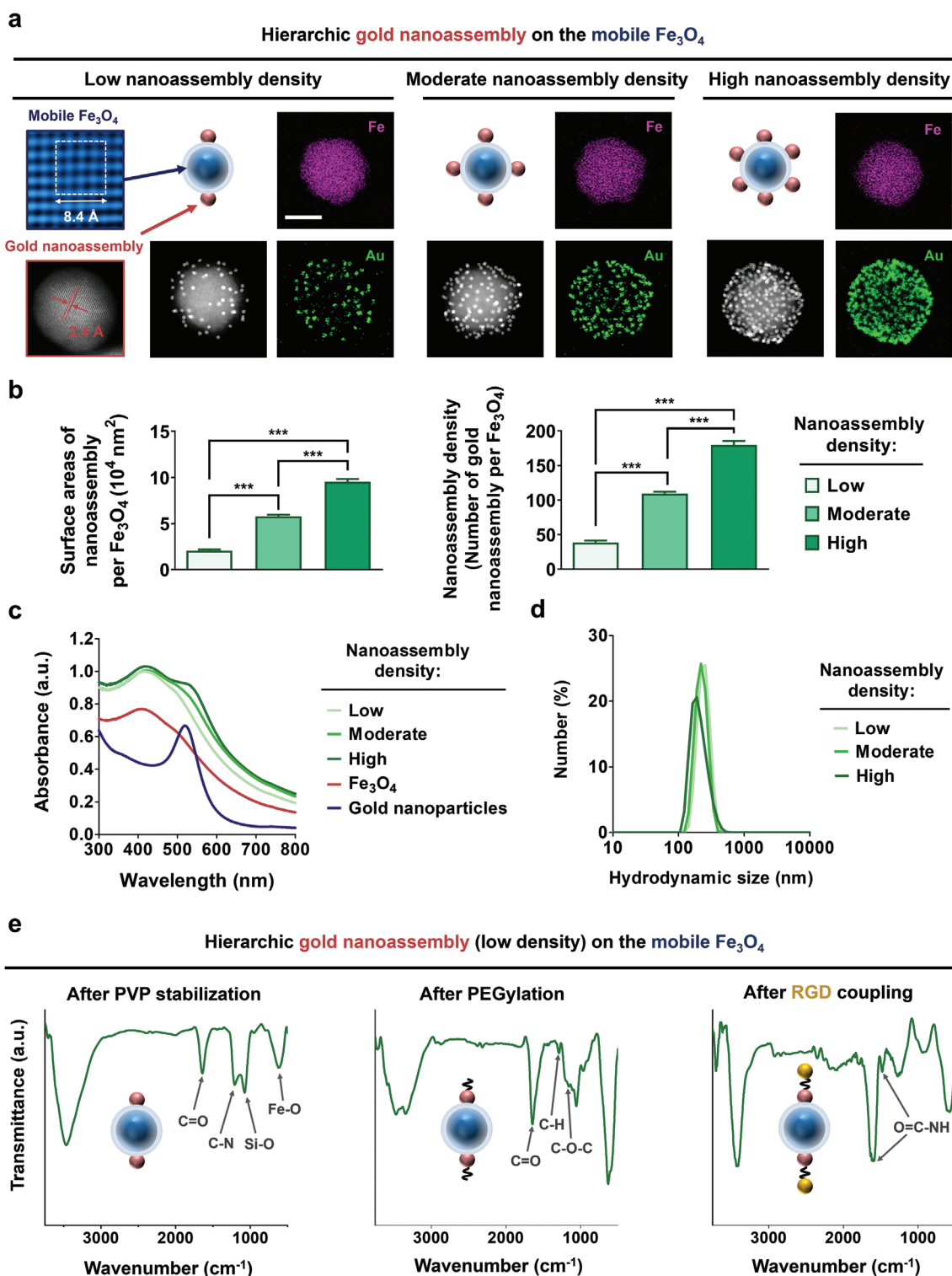
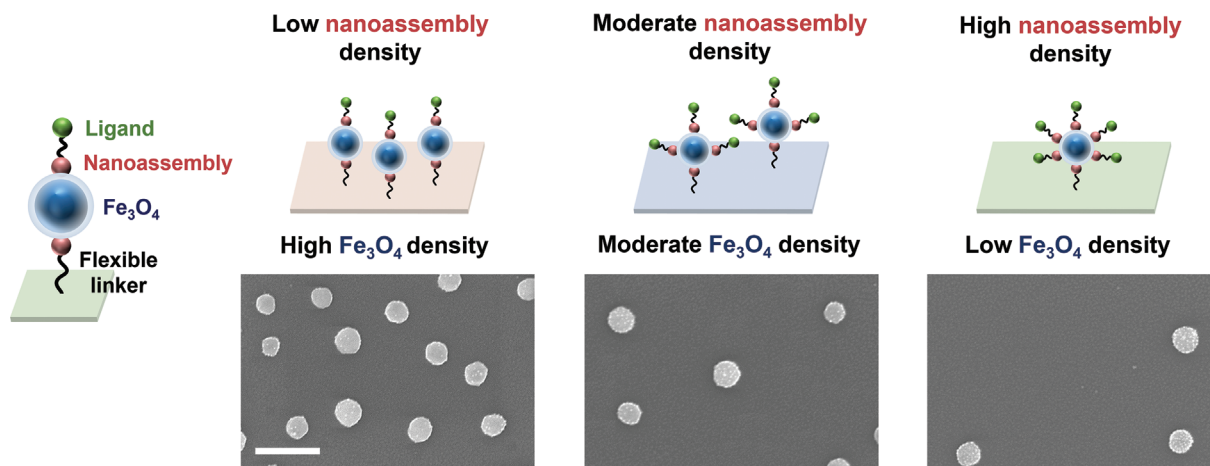


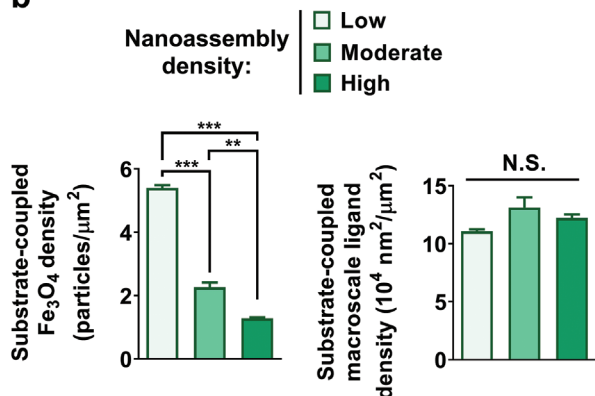
Figure 1. Methodical change of the ligand nanoassembly on the Fe_3O_4 . a) Atomic-scale characterization of the Fe_3O_4 and gold nanoassembly in a ligand nanoassembly via high-resolution scanning transmission electron microscopy (HR-STEM). The unit cell lattice parameter is labeled on the crystalline Fe_3O_4 . Average lattice spacing is labeled for the crystalline gold nanoassembly. Nanoscale characterization of the change of various ligand nanoassemblies (low, moderate, and high nanoassembly densities) via high-angle annular dark-field STEM (HAADF-STEM) and energy-dispersive X-ray spectroscopy (EDS) mapping. Scale bar: 100 nm. Fe and Au elements represent the Fe_3O_4 and gold nanoassembly, respectively. b) Quantifications of surface areas and densities of the nanoassembly per Fe_3O_4 in nanostructures. c) UV-vis absorbance spectra of the gold nanoparticles, the Fe_3O_4 nanoparticles, and various nanoassemblies. d) Dynamic light scattering of the size distribution in various nanoassemblies. e) Fourier transform infrared spectra of the nanoassembly (at low nanoassembly density) after polyvinylpyrrolidone stabilization, tethering of the flexible linker, the grafting of the amino-RGD peptide. Each absorption peak was assigned to chemical bonds that emerged after the serial chemical functionalization. *** $p < 0.001$.

a

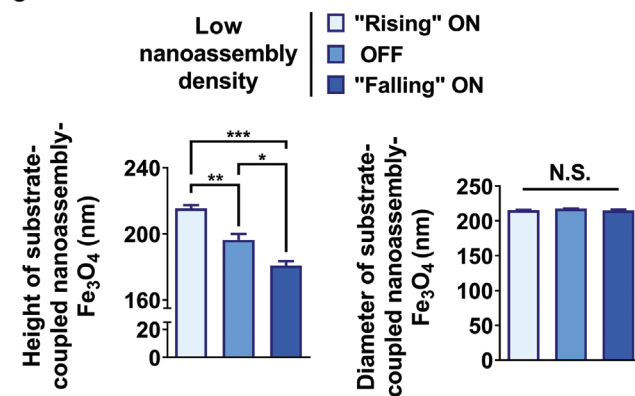
Substrate-coupled mobile Fe_3O_4 presenting ligand-nanoassembly



b



c



d

Magnetic bidirectional motion of hierarchic ligand-bearing nanoassembly

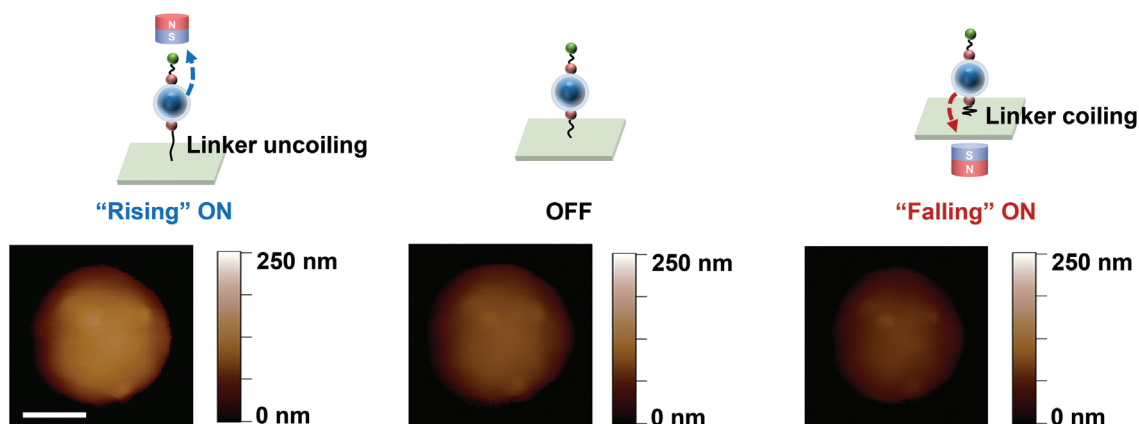


Figure 2. Remote control of the movement of various ligand nanoassemblies at a constant macroscale ligand density. a) Schematics and scanning electron microscopy (SEM) images of various ligand nanoassemblies (low, moderate, and high nanoassembly densities) on the Fe_3O_4 flexibly grafted to the substrate. Scale bar: 500 nm. b) Calculation of the substrate-grafted Fe_3O_4 density and macroscale ligand surface density. c) Quantification of the average height and diameter of the ligand nanoassemblies on the Fe_3O_4 (low nanoassembly density) based on d) the images acquired by in situ magnetic atomic force microscopy (AFM). Serial in situ magnetic AFM imaging was conducted on identical areas of the ligand nanoassemblies after placing a permanent magnet at the upper side of the substrate to induce linker-stretching-mediated rising movement ("Rising" ON) of the ligand nanoassemblies or at the lower side of the substrate to induce linker-compression-mediated falling movement ("Falling" ON) of the ligand nanoassemblies or without a magnet ("OFF"). Scale bar: 100 nm. * $p < 0.05$, ** $p < 0.01$, and *** $p < 0.001$.

and 2175 nm with no significant differences) confirm that no intrinsic size change in ligand nanoassembly occurred during in situ ligand movement. In contrast, height changes of single or multiple ligand nanoassembly in the “OFF” (196.3 ± 6.1 nm), “Rising” ON (215.3 ± 3.5 nm), and “Falling” ON (180.7 ± 4.7 nm) states that were significantly different with contrast changes verified nanoscale ligand movement by magnetically attracting ligand nanoassembly to induce stretching and compression of the flexible linker (Figure S11, Supporting Information).

2.3. Modulation of Ligand Nanoassembly Density and Magnetic Stimulation Regulates Ligation-Mediated Stem Cell Adhesion

Next, we assessed the effect of changing the ligand nanoassembly density (without modulating macroscale ligand density) on the ligation-mediated focal adhesion and mechanosensing of human mesenchymal stem cells (hMSCs).^[16f,32] We passivated the substrate areas not covered by ligand nanoassembly via PEGylation. Confocal immunofluorescence imaging revealed more pronounced expression of integrin $\beta 1$ in adherent stem cells that can promote integrin-RGD ligation with increasing ligand nanoassembly density (Figure S12a, Supporting Information). We found that this enhanced ligation with increasing ligand nanoassembly density facilitated pervasive expression of paxillin clusters and development of F-actin filaments, thereby stimulating the focal adhesion and spreading of stem cells with less elongated morphology (Figure S12a,b, Supporting Information). Our results showed that stimulated focal adhesion of stem cells with increasing ligand nanoassembly density gradually strengthened the mechanosensing of the stem cells^[33] (higher nuclear localization of yes-associated protein (YAP) and transcriptional coactivator with PDZ-binding motif (TAZ) mechanotransducers (Figure S12c,d, Supporting Information). We confirmed that focal adhesion-assisted mechanosensing of stem cells is regulated specifically in response to the modulation of the integrin-specific RGD ligand nanoassembly density by control groups (Figures S13a,b and S14a,b, Supporting Information). Our findings suggest that high density of ligand nanoassembly stimulates the integrin-specific RGD ligation that promotes the focal adhesion and mechanotransduction of stem cells. We believe that our findings of high density of ligand nanoassembly on each Fe_3O_4 may display ligand nanoclustering, similar to a previous report showing that high ligand nanoclustering promotes cell adhesion.^[19,34]

Previous reports showed that RGD ligand statically grafted to a substrate via short flexible linkers (9.5 nm from the substrate) and long flexible linkers (38.2 nm from the substrate) promoted and hindered cellular adhesion, respectively.^[35] Similar to such a difference in the distance between two linkers (28.7 nm), we observed the difference in the distance between “Rising” ON (215.3 nm via flexible linker stretching) and “Falling” ON states (180.7 nm via flexible linker compression) to be 34.6 nm (Figure 2c,d), which promoted and hindered stem cell adhesion, respectively. Therefore, we suggest that “Rising” ON state via flexible linker stretching dynamically mimicked statically a long flexible linker, which inhibited integrin ligation-mediated stem cell adhesion. Similarly, we suggest that “Falling” ON state via flexible linker compression dynamically mimicked statically a

short flexible linker, which facilitated integrin ligation-mediated stem cell adhesion.

Confocal immunofluorescent images showed in the low ligand nanoassembly, high levels of paxillin expression and F-actin assembly in the “Falling” ON states and their low levels in the “OFF” and “Rising” ON states (Figure S15a,b, Supporting Information). In the high ligand nanoassembly density, high level of stem cell adhesion was observed in the “OFF” and “Falling” ON states whereas low level of stem cell adhesion was observed in the “Rising” ON state (Figure S16a,b, Supporting Information). We also found that 18 h is the minimal time for effective magnetic stimulation of the stem cell adhesion and mechanotransduction (Figures S17a,b and S18a,b, Supporting Information). Our results demonstrated that the magnetic control of rising and falling movement of the ligand nanoassembly hinders and intensifies the integrin ligation-assisted focal adhesion and spreading, and mechanosensing (nuclear localization of TAZ and YAP mechanotransducers) of stem cells, respectively (Figure 3a; Figures S19 and S20a,b, Supporting Information). We also found that the use of linear RGD instead of cyclic RGD (used in this study) remains effective for regulating stem cell adhesion in our system (Figures S21 and S22a,b, Supporting Information). Magnetic control of nanoassembly necessitates the tethering of the integrin-specific RGD ligand to the nanoassembly to efficiently regulate focal adhesion and mechanosensing of stem cells (Figures S23a,b and S24a,b, Supporting Information). We performed in situ magnetic confocal microscopy imaging of reversible stem cell adhesion. We found that spread stem cells that had initially adhered to the ligand nanoassembly (high nanoassembly density) in “OFF” state exhibited gradual shrinkage into smaller round cells in “Rising” ON state after 6 h, suggesting reversible cell adhesion (Movie S1, Supporting Information).

2.4. The Magnetic Control and Density of Ligand Nanoassembly Regulates the Mechanotransduction-Mediated Stem Cell Differentiation

Controlling elastic movement of cell-adhesive ECM proteins has been shown to stimulate focal adhesion kinase (FAK), which mediates osteogenic differentiation of stem cells.^[7a,36] Therefore, we examined whether ligand movement can regulate mechanosensing-mediated osteogenic differentiation of stem cells.^[33,37] Confocal immunofluorescent imaging showed that the nuclear translocation of RUNX2 and alkaline phosphatase (ALP) fluorescence intensities per cell was significantly enhanced by “Falling” ON state compared to “OFF” state in low ligand nanoassembly group (Figure 3b,c; Figure S25, Supporting Information). This trend was found to be consistent in upregulating the expression of these osteogenic genes (ALP and RUNX2) and stimulating mature osteoblast-specific osteocalcin (Figure 3c; Figures S26 and S27a,b, Supporting Information). These results are also in accordance with the stimulated focal adhesion and mechanotransduction of stem cells via “Falling” ON state compared to the “OFF” state in the low ligand nanoassembly group (Figure 3a). In striking contrast, confocal immunofluorescent imaging showed that the nuclear translocation of RUNX2 and the expression of ALP and osteocalcin

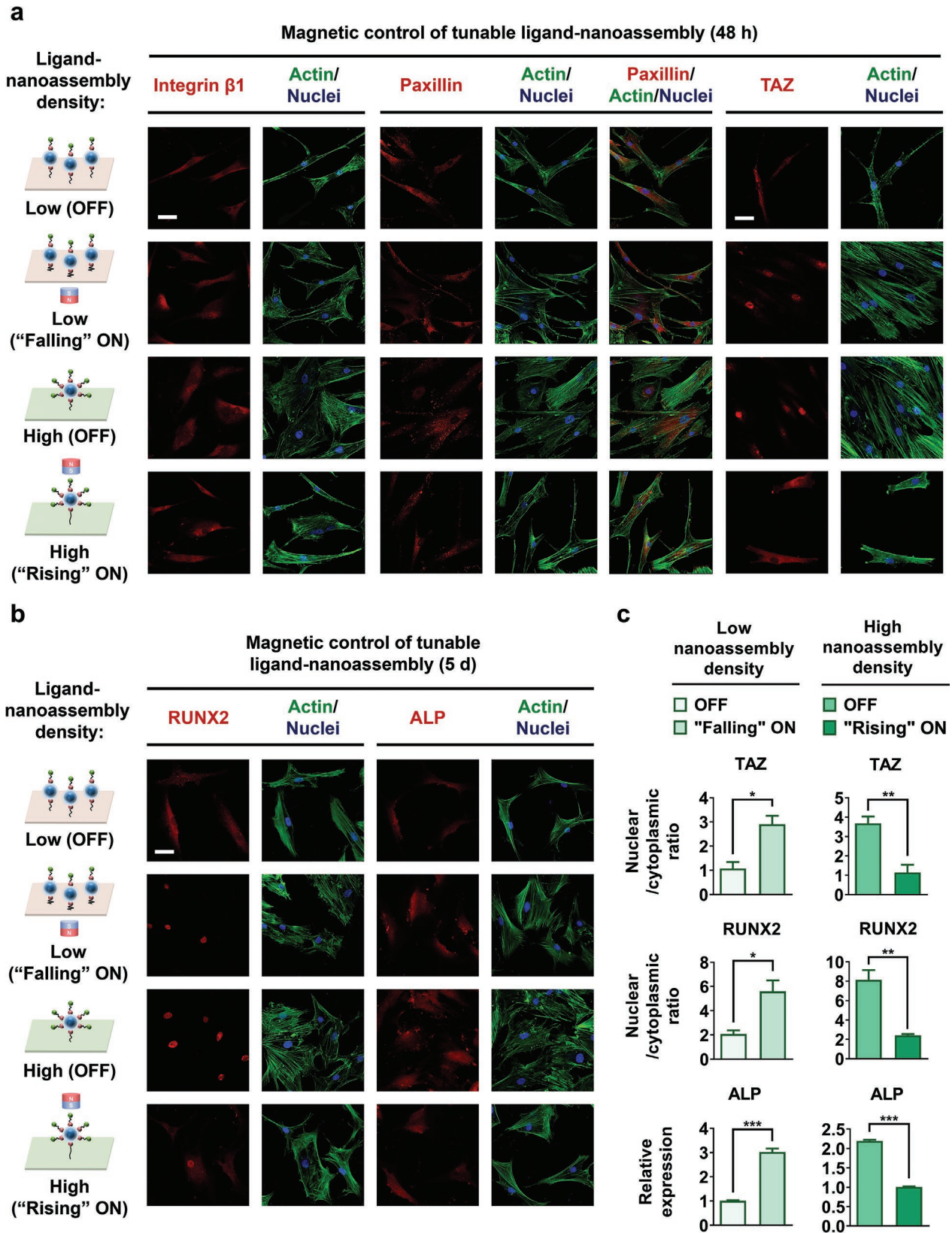
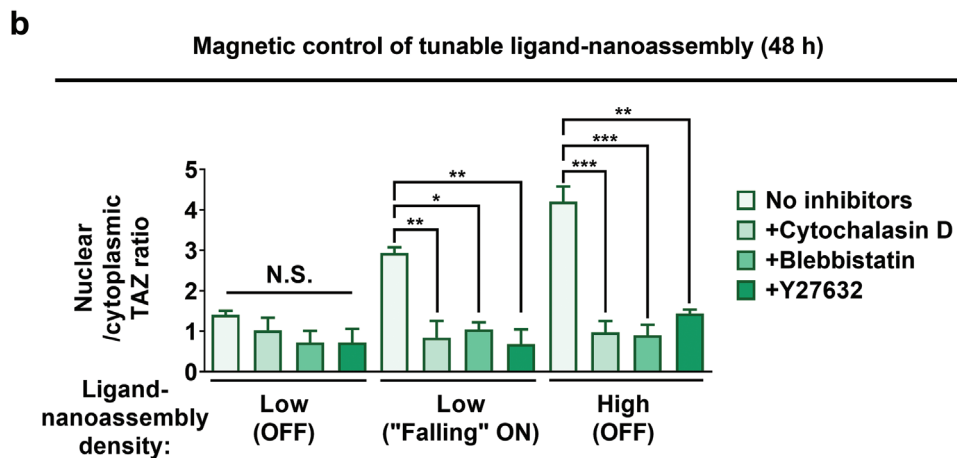
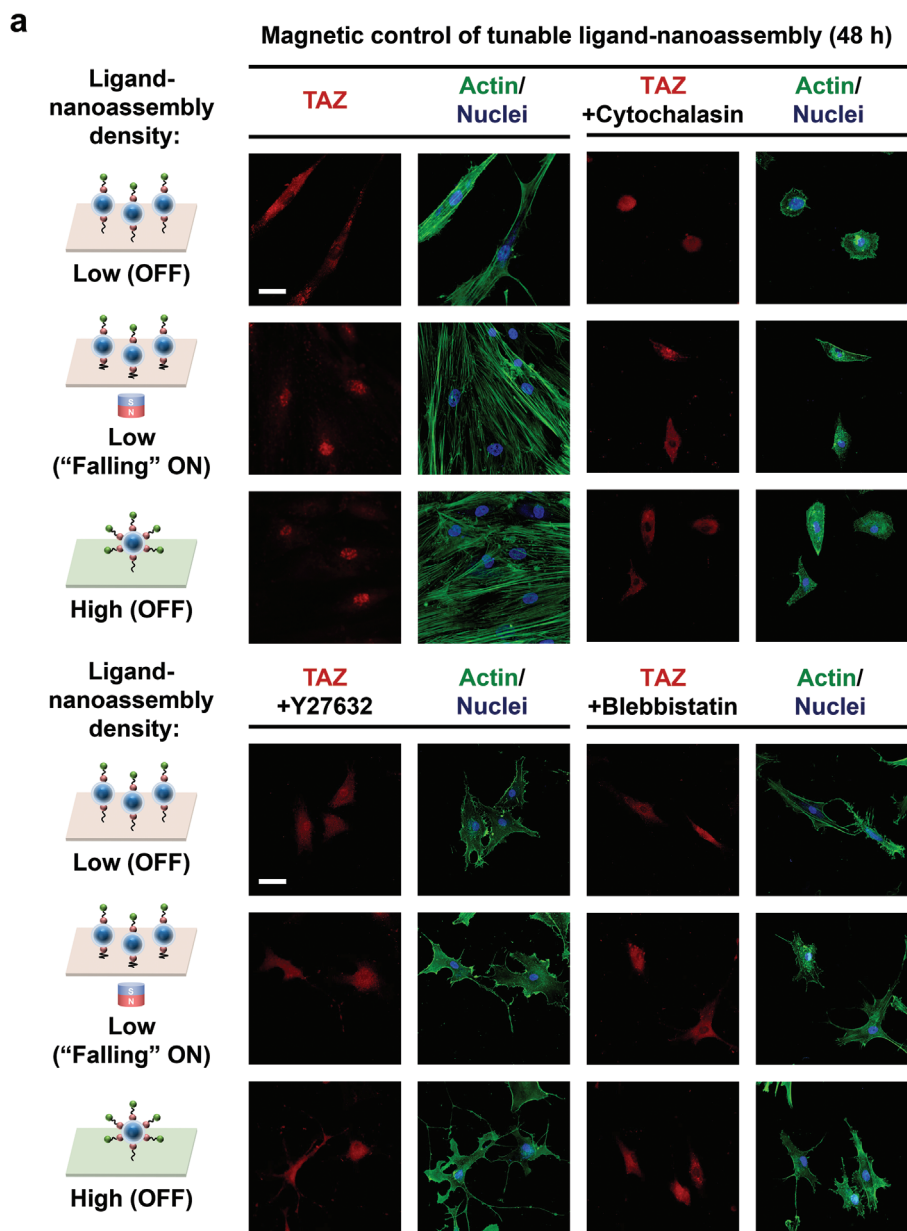


Figure 3. Magnetic control of the movement of ligand nanoassemblies oppositely regulates the adhesion and differentiation of stem cells. a) Confocal immunofluorescent images of a) integrin $\beta 1$, paxillin, and TAZ and b) RUNX2 and ALP co-stained with F-actin and 4',6-diamidino-2-phenylindole (DAPI) (nuclei) in adhered stem cells on the ligand nanoassembly (low and high densities) in the "OFF" state as well as the magnetic "Rising" ON and "Falling" ON states with c) quantification of the nuclear localization of TAZ and RUNX2 as well as ALP gene expression. Scale bar: 50 μm . * $p < 0.05$, ** $p < 0.01$, and *** $p < 0.001$.



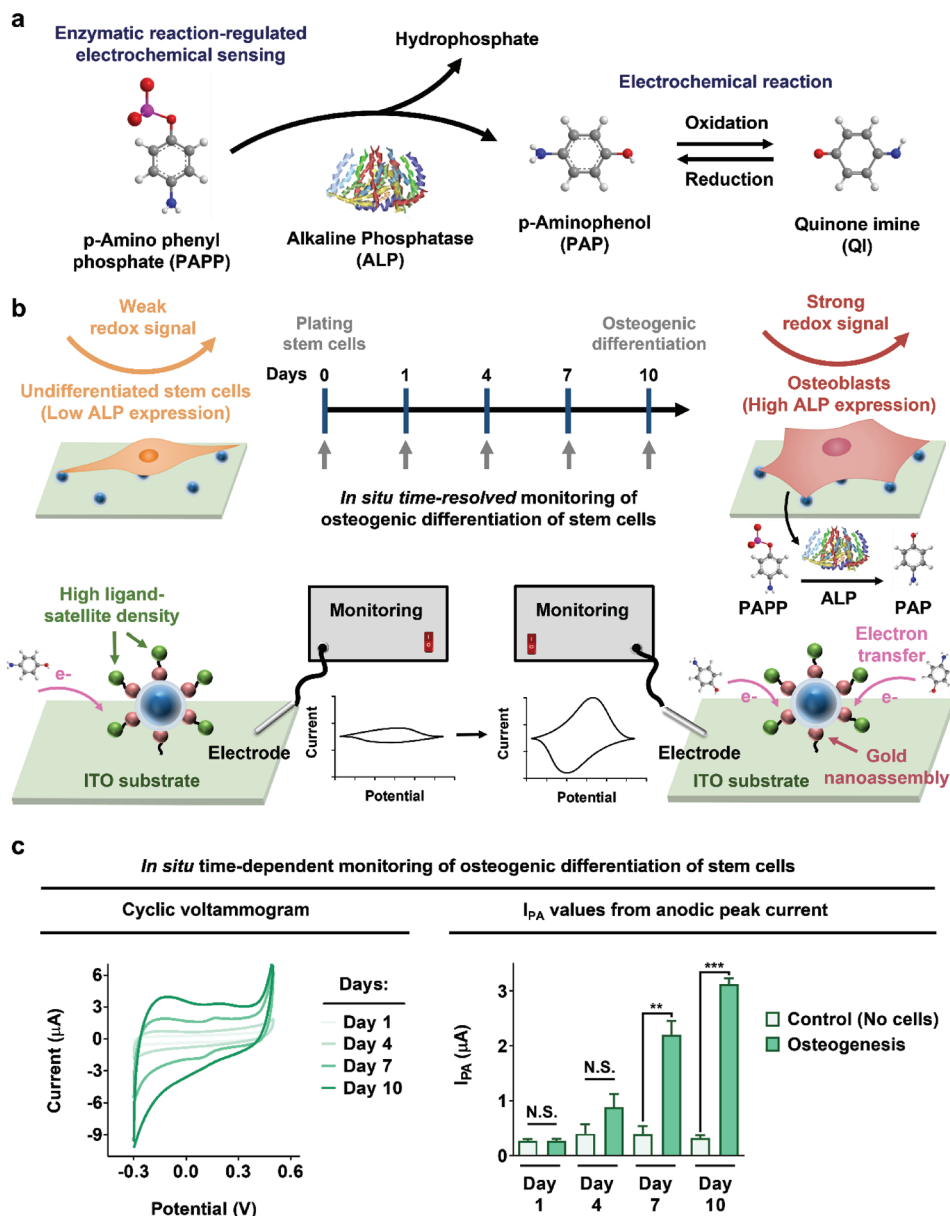


Figure 5. Ligand nanoassembly platform is versatile in enabling the in situ real-time monitoring of stem cell differentiation. a) Schematic presentation of the enzymatic reaction-regulated electrochemical sensing using alkaline phosphate (ALP) to mediate the redox reaction monitored through cyclic voltammetry (CV). b) The electroconductive indium–tin oxide (ITO) substrate presenting the ligand nanoassembly at high gold nanoassembly density facilitates the gold nanoassembly-mediated electrochemical reaction regulated by ALP produced as a result of the osteogenic differentiation of the stem cells. c) Cyclic voltammogram and calculated I_{PA} (anodic peak current) values for in situ time-dependent monitoring of stem cell differentiation. Control experiments in the absence of cells were also conducted. Data are expressed as the mean \pm standard error ($n = 3$). ** $p < 0.01$ and *** $p < 0.001$.

were significantly hindered by “Rising” ON state compared to “OFF” state in high ligand nanoassembly group (Figure 3b,c; Figures S25 and S27, Supporting Information). This trend cor-

responds to the impeded focal adhesion and mechanotransduction of stem cells via “Rising” ON state compared to “OFF” state in high ligand nanoassembly group (Figure 3a,b). We also

Figure 4. The adhesion-mediated stem cell mechanosensing is facilitated by both high density and low vertical distance of the ligand nanoassembly. a) Confocal immunofluorescent images of TAZ co-stained with F-actin and DAPI (nuclei) and b) consequent quantification analysis of the nuclear localization of TAZ in adhered stem cells after 48 h of culturing on the ligand nanoassembly (in the “OFF” state and the magnetic “Falling” ON state at low density and the “OFF” state at high density). Stem cells were cultured in the presence and absence of specific inhibitors for actin polymerization (cytochalasin D), ROCK (Y27632), or myosin II (blebbistatin). Scale bar: 50 μm . Data are depicted as mean \pm standard error ($n = 20$). * $p < 0.05$, ** $p < 0.01$, and *** $p < 0.001$.

examined sole effect of applying a magnetic field on stem cell differentiation and found poor stem cell adhesion and differentiation in all of the groups, which indicates that the magnetic field alone does not efficiently drive stem cell adhesion and differentiation (Figure S28a,b, Supporting Information). This evidence proves that magnetic manipulation of rising and falling movements of ligand nanoassembly efficiently impede and intensify mechanosensing-mediated stem cell differentiation,

respectively.^[38] Furthermore, the enhanced mechanotransduction signals observed in high density and “Falling” ON groups were hindered by inhibiting actin polymerization, rho-associated protein kinase (ROCK), or myosin II (Figure 4a,b; Figure S29a,b, Supporting Information). Collectively, actin polymerization, ROCK, and myosin II are required to efficiently induce the adhesion-dependent mechanosensing of stem cells in the high density and “Falling” ON groups.

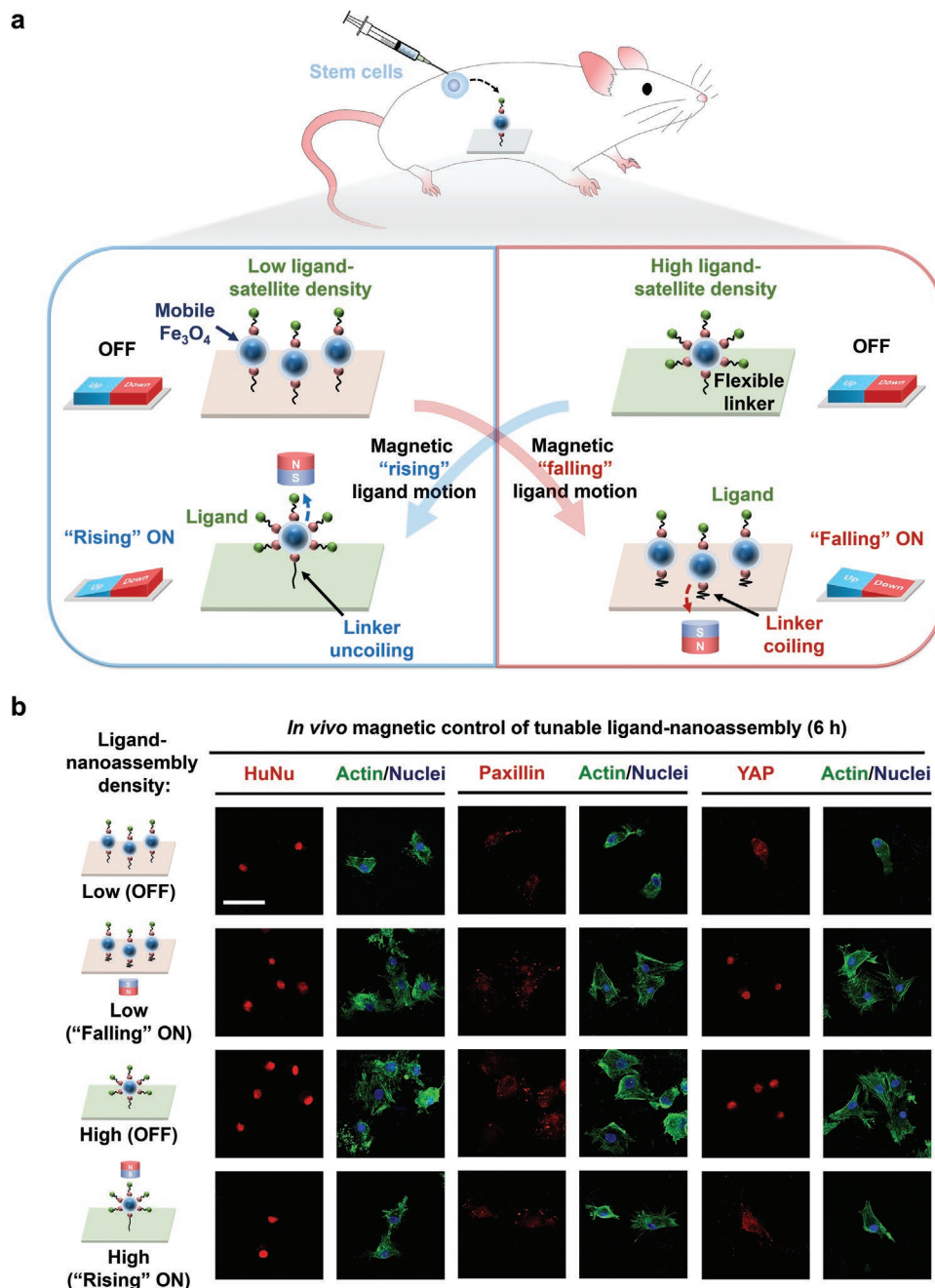


Figure 6. High density and low vertical distance of the ligand nanoassembly facilitate focal adhesion-mediated mechanosensing of stem cells *in vivo*. a) Schematic presentation and b) confocal immunofluorescent images against human-specific HuNu, paxillin, and YAP co-stained with F-actin and DAPI (nuclei) in adhered stem cells at 6 h after subcutaneous implantation of the ligand nanoassembly presenting substrate and injecting hMSCs onto the implanted substrate. Following implantation and injection, a magnet was placed on the skin on the backs (upper side for “Rising” ON) or abdomens (lower side for “Falling” ON) of the mice or without the magnet (“OFF”). Scale bar: 50 μ m.

The materials that are remotely controllable can also be used to monitor real-time changes in stem cell differentiation.^[36] We tested the feasibility of in situ monitoring of stem cells in high ligand nanoassembly on electroconductive substrate by exploiting gold nanoassembly-mediated electrochemical reaction using a three-electrode system (Figure S30a,b, Supporting Information). ALP-based redox reaction via cyclic voltammetry measurements was employed to detect time-resolved osteogenic differentiation of stem cells that produce ALP (Figure 5a–c). We are more comprehensively exploring the possibility of noninvasively monitoring stem cell differentiation under magnetic movements.

2.5. In Vivo Remote Control and Density of the Ligand Nanoassembly Regulate the Focal Adhesion-Mediated Stem Cell Mechanotransduction

Native bone exhibits RGD ligand-presenting collagen in nanostructures that dynamically regulate the adhesion and differentiation of stem cells.^[6a] We further examined whether this material of regulating stem cell responses can be translated into in vivo microenvironment. It has recently been reported that Fe₃O₄-based nanomaterials do not exhibit toxicity, suggesting their safe use.^[9,39] We subcutaneously implanted the substrate presenting ligand nanoassembly into balb/c nude mice and injected hMSCs onto the implant (Figure 6a). We either placed the magnet on the backs (upper side) or abdomens (lower side) of the mice to induce rising (“Rising” ON) or falling (“Falling” ON) movement of ligand nanoassembly or did not place the magnet (“OFF”).

After retrieving the implant, confocal immunofluorescence imaging revealed that the number of adherent cells exhibiting the number of co-localized human-specific nuclear antigen (HuNu) and nuclei (suggesting the number of injected hMSCs), focal adhesion, and mechanotransduction significantly diminished by “Rising” ON state compared to “OFF” state in high density of ligand nanoassembly (Figure 6b; Figure S31, Supporting Information). In contrast, we found that “Falling” ON state significantly elevated the number of adherent hMSCs, focal adhesion, and mechanotransduction compared to “OFF” state in low density of ligand nanoassembly. We confirmed in vivo stability of the implanted substrate presenting the ligand nanoassembly (Figure S32a,b, Supporting Information). Taken together, high density and remotely controllable falling movement of ligand nanoassembly effectively facilitate focal adhesion-mediated mechanosensing of stem cells in vivo, suggesting their safe and on-demand use in regenerative therapies.

3. Conclusion

We changed the density of the assembled ligand-presenting gold nanoparticles on the Fe₃O₄ in the nanostructures and flexibly grafted them to substrate via a flexible linker while maintaining the macroscale ligand density invariant. We showed that high and low ligand nanoassembly densities promote and hinder the mechanosensing-aided differentiation of stem cells, respectively. Magnetic control of rising ligand movement

(increasing vertical ligand distance) and falling ligand movement (decreasing vertical ligand distance) impeded and facilitated focal adhesion-mediated mechanotransduction of stem cells, respectively, both in vitro and in vivo, and resultant differentiation. Changing combination of dimensions, shapes, and biomimetic ligands in the design of ligand-presenting nanoassembly can nontoxically and remotely regulate stem cell responses to advance regenerative therapy.

Supporting Information

Supporting Information is available from the Wiley Online Library or from the author.

Acknowledgements

S.L., M.S.K., and K.D.P. contributed equally to this work. This work was supported by the National Research Foundation of Korea (NRF) grant funded by the Korea government (MSIT) (Grant Nos. 2020R1C1C1011038, 2019R1A2C3006587, and 2021R11A1A101050661) and supported by a Korea University Grant. This work was supported by the Technology Innovation Program (N0002310) funded by the Ministry of Trade, Industry and Energy (MOTIE, Korea). HAADF-STEM imaging was carried out with the support of the Korea Basic Science Institute. The authors also made use of the EPIC facility at Northwestern University’s NUANCE Center, which received support from the Soft and Hybrid Nanotechnology Experimental (SHyNE) Resource (NSF ECCS-1542205), the MRSEC IRG2 program (NSF DMR-1720139) at the Materials Research Center, the International Institute for Nanotechnology (IIN), the Keck Foundation, and the State of Illinois, through the IIN. K.-B.L. would like to acknowledge the partial financial support from the NSF (CBET-1803517) and NSF R01 (1R01DC016612).

Conflict of Interest

The authors declare no conflict of interest.

Data Availability Statement

Research data are not shared.

Keywords

ligand nanoassembly, magnetic control, stem cell differentiation, real-time differentiation monitoring

Received: May 18, 2021

Revised: July 4, 2021

Published online:

- [1] D. C. Kirouac, C. Ito, E. Csaszar, A. Roch, M. Yu, E. A. Sykes, G. D. Bader, P. W. Zandstra, *Mol. Syst. Biol.* **2010**, *6*, 417.
- [2] H. R. C. Screen, D. A. Lee, D. L. Bader, J. C. Shelton, *Proc. Inst. Mech. Eng., Part H* **2004**, *218*, 109.
- [3] J. Cassidy, A. Hiltner, E. Baer, *Connect. Tissue Res.* **1989**, *23*, 75.
- [4] N. Reznikov, R. Shahar, S. Weiner, *Acta Biomater.* **2014**, *10*, 3815.

- [5] a) M. J. Dalby, N. Gadegaard, R. O. C. Oreffo, *Nat. Mater.* **2014**, *13*, 558; b) R. Y. Chen, L. Li, L. Feng, Y. X. Luo, M. G. Xu, K. W. Leong, R. Yao, *Biomaterials* **2020**, *230*, 119627.
- [6] a) E. Baer, J. J. Cassidy, A. Hiltner, *Pure Appl. Chem.* **1991**, *63*, 961; b) Y. Y. Li, K. L. Lam, A. D. Chen, W. Zhang, B. P. Chan, *Biomaterials* **2019**, *213*, 119210; c) I. L. M. Isa, S. A. Abbah, M. Kilcoyne, D. Sakai, P. Dockery, D. P. Finn, A. Pandit, *Sci. Adv.* **2018**, *4*, eaq0597; d) X. B. Chen, J. L. Zhang, K. T. Wu, X. H. Wu, J. Y. Tang, S. Q. Cui, D. L. Cao, R. L. Liu, C. Peng, L. Yu, J. D. Ding, *Small Methods* **2020**, *4*, 2000310.
- [7] a) C. H. Huang, M. H. Chen, T. H. Young, J. H. Jeng, Y. J. Chen, *J. Cell. Biochem.* **2009**, *108*, 1263; b) Y. Jin, J. S. Lee, J. Kim, S. Min, S. Wi, J. H. Yu, G. E. Chang, A. N. Cho, Y. Choi, D. H. Ahns, S. R. Cho, E. Cheong, Y. G. Kim, H. P. Kim, Y. Kim, D. S. Kim, H. W. Kim, Z. Quan, H. C. Kang, S. W. Cho, *Nat. Biomed. Eng.* **2018**, *2*, 522; c) L. T. Yang, S. T. D. Chueng, Y. Li, M. Patel, C. Rathnam, G. Dey, L. Wang, L. Cai, K. B. Lee, *Nat. Commun.* **2018**, *9*, 3147; d) S. Patel, S. T. D. Chueng, P. T. Yin, K. Dardir, Z. Song, N. Pasquale, K. Kwan, H. Sugiyama, K. B. Lee, *Angew. Chem., Int. Ed.* **2015**, *54*, 11983; e) V. P. Y. Ma, K. Salaita, *Small* **2019**, *15*, 1900961.
- [8] a) A. E. Nel, L. Madler, D. Velegol, T. Xia, E. M. V. Hoek, P. Somasundaran, F. Klaessig, V. Castranova, M. Thompson, *Nat. Mater.* **2009**, *8*, 543; b) Y. Kohno, T. Z. Lin, J. Pajarinen, M. Romero-Lopez, M. Maruyama, J. F. Huang, K. Nathan, Z. Y. Yao, S. B. Goodman, *J. Biomed. Mater. Res., Part B* **2019**, *107*, 2500; c) Y. J. Lin, C. C. Chen, N. W. Chi, T. Nguyen, H. Y. Lu, D. Nguyen, P. L. Lai, H. W. Sung, *Adv. Mater.* **2018**, *30*, 1705605; d) L. Yu, Y. Hou, W. Xie, J. L. C. Camacho, C. Cheng, A. Holle, J. Young, B. Trappmann, W. Zhao, M. F. Melzig, *Adv. Mater.* **2020**, *32*, 2002566; e) O. Staufer, M. Schroter, I. Platzman, J. P. Spatz, *Small* **2020**, *16*, 1906424.
- [9] X. L. Liu, S. Z. Chen, H. Zhang, J. Zhou, H. M. Fan, X. J. Liang, *Adv. Mater.* **2019**, *31*, 1804922.
- [10] a) B. S. Gomes, B. Simoes, P. M. Mendes, *Nat. Rev. Chem.* **2018**, *2*, 0120; b) Y. Kim, H. Choi, J. E. Shin, G. Bae, R. Thangam, H. Kang, *View* **2020**, *1*, 20200029; c) T. Kang, Y. G. Kim, D. Kim, T. Hyeon, *Coord. Chem. Rev.* **2020**, *403*, 213092.
- [11] a) F. M. Wang, Y. Zhang, Z. Du, J. S. Ren, X. G. Qu, *Nat. Commun.* **2018**, *9*, 1209; b) H. F. Zhou, H. M. Yan, Y. Hu, L. E. Springer, X. X. Yang, S. A. Wickline, D. P. J. Pan, G. M. Lanza, C. T. N. Pham, *ACS Nano* **2014**, *8*, 7305; c) L. F. Kadem, M. Holz, K. G. Suana, Q. Li, C. Lamprecht, R. Herges, C. Selhuber-Unkel, *Adv. Mater.* **2016**, *28*, 1799; d) H. Rabie, Y. X. Zhang, N. Pasquale, M. J. Lagos, P. E. Batson, K. B. Lee, *Adv. Mater.* **2019**, *31*, 1806991; e) W. Li, Z. Q. Yan, J. S. Ren, X. G. Qu, *Chem. Soc. Rev.* **2018**, *47*, 8639.
- [12] a) J. W. Kim, H. K. Jeong, K. M. Southard, Y. W. Jun, J. Cheon, *Acc. Chem. Res.* **2018**, *51*, 839; b) L. Zwi-Dantsis, B. Wang, C. Marijon, S. Zonetti, A. Ferrini, L. Massi, D. J. Stuckey, C. M. Terracciano, M. M. Stevens, *Adv. Mater.* **2020**, *32*, 1904598; c) J. R. Lee, B. W. Park, J. Kim, Y. W. Choo, H. Y. Kim, J. K. Yoon, H. Kim, J. W. Hwang, M. Kang, S. P. Kwon, S. Y. Song, I. O. Ko, J. A. Park, K. Ban, T. Hyeon, H. J. Park, B. S. Kim, *Sci. Adv.* **2020**, *6*, eaaz0952; d) Y. Lim, S. H. Noh, T. H. Shin, J. U. Lee, D. Lungerich, J. H. Lee, J. Cheon, *Nano Lett.* **2021**, *21*, 3649.
- [13] a) W. Li, Z. W. Chen, L. Zhou, Z. H. Li, J. S. Ren, X. G. Qu, *J. Am. Chem. Soc.* **2015**, *137*, 8199; b) D. D. Li, Y. C. Ma, J. Z. Du, W. Tao, X. J. Du, X. Z. Yang, J. Wang, *Nano Lett.* **2017**, *17*, 2871.
- [14] a) T. T. Lee, J. R. Garcia, J. I. Paez, A. Singh, E. A. Phelps, S. Weis, Z. Shafiq, A. Shekaran, A. del Campo, A. J. Garcia, *Nat. Mater.* **2015**, *14*, 352; b) A. N. Ramey-Ward, H. Q. Su, K. Salaita, *ACS Appl. Mater. Interfaces* **2020**, *12*, 35903; c) Y. Tao, H. F. Chan, B. Y. Shi, M. Q. Li, K. W. Leong, *Adv. Funct. Mater.* **2020**, *30*, 2005029; d) D. Kim, S. Lee, K. Na, *Small* **2021**, *17*, 2006650.
- [15] a) Y. Hou, W. Y. Xie, L. X. Yu, L. C. Camacho, C. X. Nie, M. Zhang, R. Haag, Q. Wei, *Small* **2020**, *16*, 1905422; b) J. H. Han, M. Kwak, Y. Kim, J. Cheon, *Chem. Rev.* **2018**, *118*, 6151.
- [16] a) W. Zhu, J. M. Guo, Y. Ju, R. E. Serda, J. G. Croissant, J. Shang, E. Coker, J. O. Agola, Q. Z. Zhong, Y. Ping, F. Caruso, C. J. Brinker, *Adv. Mater.* **2019**, *31*, 1806774; b) R. J. C. Bose, N. Tharmalingam, F. J. G. Marques, U. K. Sukumar, A. Natarajan, Y. T. Zeng, E. Robinson, A. Bermudez, E. Chang, F. Habte, S. J. Pitteri, J. R. McCarthy, S. S. Gambhir, T. F. Massoud, E. Mylonakis, R. Paulmurugan, *ACS Nano* **2020**, *14*, 5818; c) S. Q. Yan, X. M. Zeng, Y. A. Tang, B. F. Liu, Y. Wang, X. G. Liu, *Adv. Mater.* **2019**, *31*, 1905825; d) J. Xu, S. S. Y. Lee, H. Seo, L. Pang, Y. Jun, R. Y. Zhang, Z. Y. Zhang, P. Kim, W. Lee, S. J. Kron, Y. Yeo, *Small* **2018**, *14*, 1803601; e) Q. Chen, C. Wang, X. D. Zhang, G. J. Chen, Q. Y. Hu, H. J. Li, J. Q. Wang, D. Wen, Y. Q. Zhang, Y. F. Lu, G. Yang, C. Jiang, J. Wang, G. Dotti, Z. Gu, *Nat. Nanotechnol.* **2019**, *14*, 89; f) B. Meckes, R. J. Banga, S. T. Nguyen, C. A. Mirkin, *Small* **2018**, *14*, 1702909; g) M. Pagel, R. Hassert, T. John, K. Braun, M. Wessler, B. Abel, A. G. Beck-Sickinger, *Angew. Chem., Int. Ed.* **2016**, *55*, 4826.
- [17] a) K. Ye, X. Wang, L. P. Cao, S. Y. Li, Z. H. Li, L. Yu, J. D. Ding, *Nano Lett.* **2015**, *15*, 4720; b) X. Wang, S. Y. Li, C. Yan, P. Liu, J. D. Ding, *Nano Lett.* **2015**, *15*, 1457; c) X. N. Liu, R. L. Liu, B. Cao, K. Ye, S. Y. Li, Y. X. Gu, Z. Pan, J. D. Ding, *Biomaterials* **2016**, *111*, 27.
- [18] J. A. Deeg, I. Louban, D. Aydin, C. Selhuber-Unkel, H. Kessler, J. P. Spatz, *Nano Lett.* **2011**, *11*, 1469.
- [19] L. Y. Koo, D. J. Irvine, A. M. Mayes, D. A. Lauffenburger, L. G. Griffith, *J. Cell Sci.* **2002**, *115*, 1423.
- [20] J. H. Huang, S. V. Grater, F. Corbellini, S. Rinck, E. Bock, R. Kemkemer, H. Kessler, J. D. Ding, J. P. Spatz, *Nano Lett.* **2009**, *9*, 1111.
- [21] C. S. Chen, M. Mrksich, S. Huang, G. M. Whitesides, D. E. Ingber, *Science* **1997**, *276*, 1425.
- [22] M. S. Bootharaju, W. Baek, S. Lee, H. Chang, J. Kim, T. Hyeon, *Small* **2020**, *17*, 2002067.
- [23] a) M. Colombo, S. Carregal-Romero, M. F. Casula, L. Gutiérrez, M. P. Morales, I. B. Böhm, J. T. Heverhagen, D. Prospero, W. J. Parak, *Chem. Soc. Rev.* **2012**, *41*, 4306; b) X. P. Duan, C. Chan, W. B. Lin, *Angew. Chem., Int. Ed.* **2019**, *58*, 670; c) Y. Lim, C. H. Lee, C. H. Jun, K. Kim, J. Cheon, *J. Am. Chem. Soc.* **2020**, *142*, 9130; d) X. L. Wu, C. L. Hao, L. G. Xu, H. Kuang, C. L. Xu, *Small* **2020**, *16*, 1905734.
- [24] a) S. Min, Y. S. Jeon, H. J. Jung, C. Khatua, N. Li, G. Bae, H. Choi, H. Hong, J. E. Shin, M. J. Ko, H. S. Ko, I. Jun, H. E. Fu, S. H. Kim, R. Thangam, J. J. Song, V. P. Dravid, Y. K. Kim, H. Kang, *Adv. Mater.* **2020**, *32*, 2004300; b) S. Min, Y. S. Jeon, H. Choi, C. Khatua, N. Li, G. Bae, H. J. Jung, Y. Kim, H. Hong, J. Shin, M. J. Ko, H. S. Ko, T. Kim, J. H. Moon, J. J. Song, V. P. Dravid, Y. K. Kim, H. Kang, *Nano Lett.* **2020**, *20*, 7272.
- [25] a) S. Min, M. J. Ko, H. J. Jung, W. Kim, S. B. Han, Y. Kim, G. Bae, S. Lee, R. Thangam, H. Choi, N. Li, J. E. Shin, Y. S. Jeon, H. S. Park, Y. J. Kim, U. K. Sukumar, J. J. Song, S. K. Park, S. H. Yu, Y. C. Kang, K. B. Lee, Q. Wei, D. H. Kim, S. M. Han, R. Paulmurugan, Y. K. Kim, H. Kang, *Adv. Mater.* **2021**, *33*, 2008353; b) G. Bae, Y. S. Jeon, M. J. Ko, Y. Kim, S. B. Han, R. Thangam, W. Kim, H. J. Jung, S. Lee, H. Choi, S. Min, H. Hong, S. Park, S. Y. Kim, K. D. Patel, N. Li, J. E. Shin, B. C. Park, H. S. Park, J. H. Moon, Y. J. Kim, U. K. Sukumar, J. J. Song, S. Y. Kim, S. H. Yu, Y. C. Kang, S. Park, S. M. Han, D. H. Kim, K. B. Lee, Q. Wei, L. M. Bian, R. Paulmurugan, Y. K. Kim, H. Kang, *Adv. Funct. Mater.* **2021**, *31*, 2103409.
- [26] a) H. Choi, G. Bae, C. Khatua, S. Min, H. J. Jung, N. Li, I. Jun, H. W. Liu, Y. Cho, K. H. Na, M. Ko, H. Shin, Y. H. Kim, S. Chung, J. J. Song, V. P. Dravid, H. Kang, *Adv. Funct. Mater.* **2020**, *30*, 2001446; b) C. Khatua, S. Min, H. J. Jung, J. E. Shin, N. Li, I. Jun, H. W. Liu, G. Bae, H. Choi, M. J. Ko, Y. S. Jeon, Y. J. Kim, J. Lee, M. Ko, G. Shim, H. Shin, S. Lee, S. Chung, Y. K. Kim, J. J. Song, V. P. Dravid, H. Kang, *Nano Lett.* **2020**, *20*, 4188.
- [27] S. H. D. Wong, X. Xu, X. Chen, Y. Xin, L. M. Xu, C. H. N. Lai, J. Oh, W. K. R. Wong, X. M. Wang, S. S. Han, W. X. You, X. T. Shuai, N. Wong, Y. H. Tan, L. Duan, L. M. Bian, *Nano Lett.* **2021**, *21*, 3225.

- [28] D. S. H. Wong, J. N. Li, X. H. Yan, B. Wang, R. Li, L. Zhang, L. M. Bian, *Nano Lett.* **2017**, *17*, 1685.
- [29] S. H. D. Wong, W. K. R. Wong, C. H. N. Lai, J. Oh, Z. Li, X. Y. Chen, W. H. Yuan, L. M. Bian, *Nano Lett.* **2020**, *20*, 3207.
- [30] G. Q. Pan, S. Shinde, S. Y. Yeung, M. Jakstaite, Q. J. Li, A. G. Wingren, B. Sellergren, *Angew. Chem., Int. Ed.* **2017**, *56*, 15959.
- [31] J. Y. Kim, J. Yeom, G. P. Zhao, H. Calcaterra, J. Munn, P. J. Zhang, N. Kotov, *J. Am. Chem. Soc.* **2019**, *141*, 11739.
- [32] H. Jeong, J. J. Lee, J. Lee, K. Na, *Small* **2020**, *16*, 2000556.
- [33] K. H. Vining, D. J. Mooney, *Nat. Rev. Mol. Cell Biol.* **2017**, *18*, 728.
- [34] H. S. Kim, X. Y. Sun, J. H. Lee, H. W. Kim, X. B. Fu, K. W. Leong, *Adv. Drug Delivery Rev.* **2019**, *146*, 209.
- [35] a) S. J. Attwood, E. Cortes, A. W. M. Haining, B. Robinson, D. Y. Li, J. Gautrot, A. D. Hernandez, *Sci. Rep.* **2016**, *6*, 34334; b) B. Trappmann, J. E. Gautrot, J. T. Connelly, D. G. Strange, Y. Li, M. L. Oyen, M. A. C. Stuart, H. Boehm, B. Li, V. Vogel, *Nat. Mater.* **2012**, *11*, 642.
- [36] J. Shin, J. H. Cho, Y. Jin, K. Yang, J. S. Lee, H. J. Park, H. S. Han, J. Lee, H. Jeon, H. Shin, S. W. Cho, *Small* **2016**, *12*, 6266.
- [37] T. C. von Erlach, S. Bertazzo, M. A. Wozniak, C. M. Horejs, S. A. Maynard, S. Attwood, B. K. Robinson, H. Autefage, C. Kallepitis, A. D. Hernandez, C. S. Chen, S. Goldoni, M. M. Stevens, *Nat. Mater.* **2018**, *17*, 237.
- [38] D. Q. Yu, M. M. Ma, Z. W. Liu, Z. F. Pi, X. B. Du, J. S. Ren, X. G. Qu, *Biomaterials* **2020**, *255*, 120160.
- [39] a) K. Maier-Hauff, F. Ulrich, D. Nestler, H. Niehoff, P. Wust, B. Thiesen, H. Orawa, V. Budach, A. Jordan, *J. Neuro-Oncol.* **2011**, *103*, 317; b) C. Y. Wang, Y. P. Xiao, W. W. Zhu, J. C. Chu, J. Xu, H. Zhao, F. Y. Shen, R. Peng, Z. Liu, *Small* **2020**, *16*, 2000589.